Granular Matter (2024) 26:25
https://doi.org/10.1007/s10035-024-01397-4

ORIGINAL REPORT

Effect of initial fabric anisotropy on cyclic liquefaction behavior of granular soils using discrete element method

Mahsa Ajam Norouzi[1] · **Ehsan Seyedi Hosseininia**[1]

Received: 20 June 2023 / Accepted: 17 January 2024

Abstract
This study employs the Discrete Element Method (DEM) to investigate the influence of initial fabric anisotropy on the cyclic liquefaction behavior of granular soils. Static and cyclic biaxial compression tests under undrained condition are simulated using two-dimensional elongated sharp-angled particles. Initial fabric anisotropy is introduced by considering a pre-defined inclined angle of elongated particles inside the sample. Results from the simulations reveal that varying fabric anisotropy affects the stress paths, resulting in a significant decrease in the maximum internal friction angle; however, the critical state internal friction angle is less affected. When subjected to cyclic loading, anisotropic samples exhibit distinct behavior influenced by initial fabric anisotropy. Comparison of the results with those of limited experiments in the literature confirms the simulations validity. The effective confining stress diminishes, leading to progressive liquefaction. The number of cycles required for initial liquefaction varies due to inherent anisotropy, and fabric anisotropy causes a shift in the concentration of compression or extension strains within the samples. Lower values of cyclic stress ratio amplifies the influence of inherent anisotropy on excess pore water pressure ratios. In addition to stress approach, the strain-based liquefaction resistance is also investigated by defining double amplitude strain values. It is found that when the double strain level is relatively small, the impact of inherent anisotropy becomes more noticeable. This study enhances the understanding of the role of initial fabric anisotropy in cyclic liquefaction behavior and provides insights for engineering design and mitigation strategies in seismic-prone areas.

Keywords Cyclic liquefaction · Granular soils · Initial fabric anisotropy · Discrete Element Method · Undrained condition · Stress path · Polygonal particles

1 Introduction

Soil liquefaction, a significant phenomenon observed in sandy soil during earthquakes, has garnered considerable attention from geotechnical engineers due to its destructive impact on earth structures. The liquefaction phenomenon can occur in response to both static and cyclic loading, known as static and cyclic liquefaction, resulting in the accumulation of large strains. To enhance earthquake hazard analysis and mitigate structural damage, a deeper understanding of cyclic liquefaction is necessary. When undrained sand undergoes cyclic loading, the effective stress gradually diminishes while the pore water pressure increases. Initially, deformations progress at a relatively slow pace during loading; however, as the loading cycles intensify, the rate of deformation accelerates, leading to the onset of liquefaction. The primary cause is the reduction of effective soil stress, eventually approaching zero.

The liquefaction behavior of sands can be influenced by multiple factors, including the grain size, grain geometry, angularity, soil porosity, soil fabric, and initial effective stress. Among the mentioned factors, the shape of the particles plays a crucial role in determining the strength of the granular soil and, consequently, its susceptibility to liquefaction. In natural conditions, granular soil particles can exhibit elongated, non-circular, and angular geometries. Kandasami and Murthy [1] conducted a study to examine how the shape of grains influences the mechanical behavior of granular soil. They discovered that soil samples containing angular particles tend to contract, whereas samples containing spherical particles tend to expand. In a separate study, Ashmawy et al.

✉ Ehsan Seyedi Hosseininia
eseyedi@um.ac.ir

[1] Department of Civil Engineering, Faculty of Engineering, Ferdowsi University of Mashhad, Mashhad, Iran

Published online: 05 February 2024

[2] employed a numerical approach to investigate both the liquefaction potential and the impact of grain geometry on the cyclic response of soil. They conducted undrained cyclic shear tests on particle assemblies with varying degrees of sharpness. The findings from this study revealed that both the shape and density of the particles significantly influence the susceptibility of the sample to liquefaction. Additionally, Keramatikerman and Chegenizadeh [3] explored the impact of particle shape on static liquefaction through static triaxial compression tests. In this study, the researchers utilized a naturally occurring sand composed of rounded particles. To investigate the effects of particle shape, they crushed some of the sand particles, creating sharp-edged particles. The experiments were then conducted using the natural sand, crushed sand, and a combination of the two. The results of the tests revealed contrasting behaviors in shear response between the natural sand and crushed sand. Notably, an increase in the proportion of crushed particles led to enhanced resistance against liquefaction, along with significant alterations observed in the shear response of the samples.

Apart from the particle shape, the arrangement of particles, known as soil fabric, can also impact the resistance behavior of granular soil. As a result, laboratory findings suggest a significant correlation between the liquefaction resistance of sands and the soil fabric [1, 4–15]. The term "fabric" refers to how particles are arranged in relation to each other, including their shape and the distribution of pores within the particle set. Typically, soil fabric exhibits anisotropy, meaning that it is not uniform in all directions. In nature, during the process of sediment formation, particles tend to align themselves in a specific direction. This alignment is primarily influenced by gravitational forces acting on the particles. As a result, the soil fabric becomes oriented and exhibits preferred directions of particle arrangement. An illustration of this phenomenon can be found in the work of Oda et al. [6], who noted that fabric anisotropy resulting from the parallel alignment of particles is commonly observed in sands found in rivers, beaches, and coastal hills. Notably, this type of anisotropy can also be present in artificially deposited sand layers. The anisotropy that arises from the settling process and gravitational forces is referred to as inherent anisotropy. Previous studies have demonstrated that fabric anisotropy in soil can lead to different responses under loading conditions. Researchers such as Arthur and Menzies [4] and Oda [5] conducted experiments involving sand samples with varying layering directions to investigate the impact of inherent anisotropy. Using a triaxial compression machine, they observed that the initial direction in which the sand was placed had a significant influence on the deviatoric stress exhibited by the sample. Oda [5] demonstrated that the natural directional dependence influences both the expansion tendency of the sample and the modulus of secant deformation. According to Oda [6], who conducted experiments on sand samples, the shear strength of the soil is not consistent but varies depending on the angle at which, the particles are placed. It was observed that samples loaded perpendicular to the plane of the particle bed exhibit greater undrained shear strength. The impact of fabric anisotropy on the mechanical properties of soil was explored by Yang et al. [11] through triaxial static compression tests conducted on sand samples prepared using different techniques. Two methods including moist tamping and dry deposition were employed for sample preparation. The findings of their study revealed that altering the sample preparation method leads to variations in the sample's behavior. Specifically, the sample prepared using the moist tamping method exhibited higher resistance to pore pressure formation and displayed a more pronounced expansion response compared to the sample prepared using the dry deposition method. Miura and Toki [7] and Sze and Yang [12] conducted both triaxial static compression tests and cyclic tests on sand samples prepared using various methods. These tests aimed to examine how fabric anisotropy influenced the overall behavior of the samples. In the triaxial compression tests, where loading was applied vertically, the researchers analyzed the impact of different preparation methods on the macroscopic response of the samples. The research findings indicated that the method of sample preparation and the resulting fabric had a significant influence on the sand's behavior during cyclic loading. Notably, the resistance to liquefaction and the expansion response of the samples varied depending on the preparation method. Miura and Toki [8] and Sze Yang [12] examined the response of undrained specimens under cyclic triaxial loading conditions. In contrast to static loading, the findings from undrained cyclic triaxial tests indicated that samples with a horizontal bed exhibited the least resistance to liquefaction. Oda et al. [10] conducted a study examining the impact of different angles of particle placement on soil samples. These angles included zero, 30, 45, 60, and 90°. The findings revealed that horizontally placed particles exhibited lower resistance to liquefaction, whereas increasing the angle of particle placement enhanced the resistance to liquefaction. Numerous studies have highlighted the significant influence of fabric anisotropy on soil strength, bearing capacity, and both elastic and plastic properties. However, the technical literature contains limited research on the correlation between excess pore water pressure generated during the initial loading cycle and liquefaction resistance [10, 16]. These studies have explored various factors such as relative density, cyclic stress ratio, sample preparation method, and effective confining stress of the soil.

Quantifying soil fabric through laboratory methods is a challenging task. However, the numerical Discrete Element Method (DEM) offers a viable solution for obtaining micro-scale details about granular aggregates. By

simulating real particles and their interactions, DEM serves as an effective tool for measuring and evaluating soil fabric. Cundall and Strack [17] developed the initial computer program, known as BALL, employing the discrete element method to model granular materials composed of circular disks in a two-dimensional setting. Another computer program called POLY was designed to simulate the behavior of polygonal particles [18]. The latter program has been developed to employ the impact of particle breakage [19, 20], model the particulate mechanism of sand production in granular assemblies with different bonding conditions [21], and also takes into account the effects of fabric anisotropy on the performance of these aggregates [22–25].

Researchers such as Sazzad and Suzuki [26], Mahmood and Iwashita [27], and Yang et al. [28] have examined the impact of soil fabric anisotropy using elliptical particles, while Seyedi Hosseininia [22, 23] focused on two-dimensional sharp particles, employing the DEM method. In this study, various placement angles were assigned to the particles in the samples, which were then subjected to one-way deviator loading. All of the aforementioned studies revealed a significant alteration in the mechanical behavior of the samples based on the initial placement angle of the particles. Moreover, it was noted that as the placement angle of the particles increased, the stress ratio of the sample decreased, resulting in a transition from expansion to contraction in the sample's behavior. The research conducted by Seyedi Hosseininia [23] found that heterogeneous samples consisting of polygonal grain particles exhibited greater shear strength in comparison to samples containing elliptical particles. The disparity in strength was attributed to the distinctive shapes of the particles. Another study conducted by Jiang et al. [29] and Lu et al. [30] examined the impact of fabric anisotropy on the mechanical properties of sand by altering the angle of the particle bed during undrained static biaxial tests, using DEM. Their findings revealed that fabric anisotropy influenced both the resistance of the samples and the internal friction angle at its peak. Numerical simulations conducted using the DEM were utilized to examine the impact of initial fabric on the resistance to liquefaction through undrained cyclic tests. The findings revealed that varying initial fabrics resulted in diverse levels of liquefaction resistance [13, 31–34]. Additionally, it was observed that the anisotropy of the fabric influenced the location of strain localization [34]. Wang et al. [35] employed numerical simulation through DEM to verify the accuracy of a constitutive model under cyclic loading. They utilized the cluster technique to generate elongated particles. Through DEM-based simulations of cyclic tests, they investigated samples with bedding plane angles of 0° and 45° and found that the initial bedding angle has a notable impact on shear strength and resistance to liquefaction.

Limited research has been conducted on the impact of fabric anisotropy on the resistance of granular soil to liquefaction, as evident from the technical literature. This article aims to explore the influence of fabric on the resistance of granular soil against cyclic liquefaction. The research employs the DEM as a numerical approach. To accomplish this, various samples of sandy soil with diverse initial fabric conditions were prepared and exposed to cyclic loading under undrained conditions, while maintaining a constant deviatoric stress range. To simplify matters, the simulation takes place in a two-dimensional environment. Previous studies have primarily utilized circular, spherical, or oval particles to create samples with inherent fabric anisotropy [13, 26–32, 34, 35]. However, in this particular research, polygonal particles are employed, reducing the required number of particles in comparison with the cluster technique. The samples' resistance to liquefaction is assessed using two distinct criteria: stress criterion (initial liquefaction) and strain criterion by defining of double amplitude strain range. Furthermore, the study aims to examine the impact of particle long axis alignment relative to the loading axis.

2 Numerical simulation of anisotropic samples

This study utilized a developed version of a computer program POLY to conduct simulations of biaxial compression tests on soil samples [19, 20, 22–25]. The program employs the DEM numerical method and considers soil particles with various shapes including irregular and convex polygons, in a two-dimensional setting. The soil samples were subjected to both static and cyclic loading conditions, and the simulations were performed under both drained and undrained conditions. Specifically, the undrained simulation of polygonal granular materials was conducted using the constant volume method in this research. This approach disregards the water surrounding the solid particles, instead simulating the undrained state by assuming both water and solid particles are incompressible and maintaining a constant total sample volume. The process of simulating the undrained biaxial compression test involves three stages: generation of soil samples, confinement of the soil samples, and applying biaxial loading (deviatoric stress).

2.1 General features

2.1.1 Particle shape definition

The shape of particles can be described as an irregular polygon, allowing for the inclusion of particles of various shapes and sizes within an ellipse. Figure 1 illustrates the overall

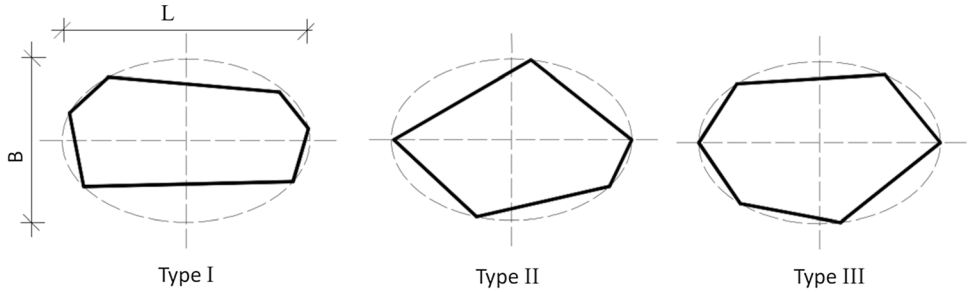

Fig. 1 Particle geometry used in the present study

Table 1 Dimensions of particles

Particle type	B (mm)	L (mm)
I, II, III	3	4.5
I, II, III	4	6
I, II, III	5	7.5

particle geometry in relation to the encompassing ellipse. This ellipse is characterized by a major axis with a length of L and a minor axis with a length of B. The dimensions of the ellipse can vary. Table 1 presents the specific properties of different soil samples, each of which contains particles conforming to this geometry. The samples analyzed in this study are uniformly graded, exhibiting a uniformity coefficient of 1.3 and a curvature coefficient of 0.89.

2.1.2 Contact model

The primary challenge in the simulation process of contacting polygonal particles is the accurate detection of contacts between these particles. For the current simulation, the overlap-area contact law [18] is utilized and the details are explained by Seyedi Hosseininia [22]. In this approach, a contact is characterized by an overlap area between the two contacting particles (A). The line connecting the intersection points of the contact surface represents the contact length (L) between the particles. The indentation length (δ) can be defined as $\delta = A/L$. Each contact force consists of both normal and tangential components with respect to the contact surface direction. The value of the normal (F_n) and tangential (Fs) contact force components are defined as $F_n = k_n\delta$ and $F_n = k_s\Delta$, where k_n and k_s represent the normal and tangential stiffness coefficients. Δ is the relative tangential displacement of the two particles along the contacting length. It is assumed that the behavior of normal contact force is elastic, while the tangential contact force behaves as frictional, and according the value is limited. This means that sliding may occur along the contact surface when $|F_s| > \mu.F_n$. Otherwise, the relationship between shear force and tangential displacement is recoverable. Here, μ is the inter-particle friction coefficient. The values of the parameters in thus study are in accordance with Table 2.

Table 2 DEM parameters used in the present study

Parameter	Unit	value
Particle density	Kg/m^3	2500
Normal spring constant ($_{kn}$)	N/m	2×10^8
Tangential spring constant (k_s)	N/m	2×10^8
inter-particle friction coefficient (μ)	–	0.5

2.1.3 Boundary conditions

In the POLY program, boundary conditions can be applied in two forms: strain-controlled and stress-controlled. In the strain-controlled mode, the boundary particles are imposed to move towards or outwards the center of the sample with a predefined velocity in a tensorial form. The horizontal and vertical components of the displacement of each boundary particle is calculated by the tensorial multiplication of the velocity tensor and the particle location vector which introduces the situation of the particle with respect to the center of the sample. This configuration is utilized in this research for the initial isotropic compression (i.e., a uniform radial displacement) to reduce the voids after the sample generation. In addition, the strain-controlled mode was implemented as an imposed displacement of boundary particles in order to simulate the upper and lower parts of the sample. In the other mode, i.e., the stress-controlled mode, the boundary particles are moved such that a desired value of stress components (in terms of a stress tensor) are formed over the total boundary and throughout the sample, accordingly. The boundary particles movement is calculated by exerting an external force whose value is obtained from the deviation of stress target and the existing stress components. In this numerical study, this configuration is utilized for the simulation of sample confinement under an isotropically-compression value of 700 kPa, which is explained in detail in Sect. 2.3. This feature was also used in the simulation of cyclic loading by defining a desired level of deviatoric stress, as explained later in Sect. 2.5. The more details of boundary condition application as well as stress and strain tensors in a granular assembly is described by Seyedi Hosseininia [23, 24].

2.2 Soil samples generation

Sample granulation involves placing particles randomly in a circular area resembling a soil sample. The initial arrangement of these particles is determined by the inclination bedding angle (α), which represents the angle between the major axis of the particle's surrounding ellipse and the horizon. Figure 2 illustrates the samples created with bedding angles α of 0, 30, 45, 60, and 90°. Each soil sample contains approximately 2000 polygonal particles. During the initial formation of the sample, particles with similar bed angles are organized within the sample space, leading to the creation of inherent anisotropy in the soil sample. Specifically, the angle at which the particles in each sample are arranged indicates the inherent anisotropy angle of the soil fabric in relation to the horizon. Apart from these samples with inherent anisotropy, a sample with an isotropic fabric has also been generated. This means that the particle angles are randomly distributed between zero and 360° within the sample. Consequently, it can be stated that the frequency of particles arranged at a specific inclination angle is equal throughout the entire sample. In other words, the overall sample's

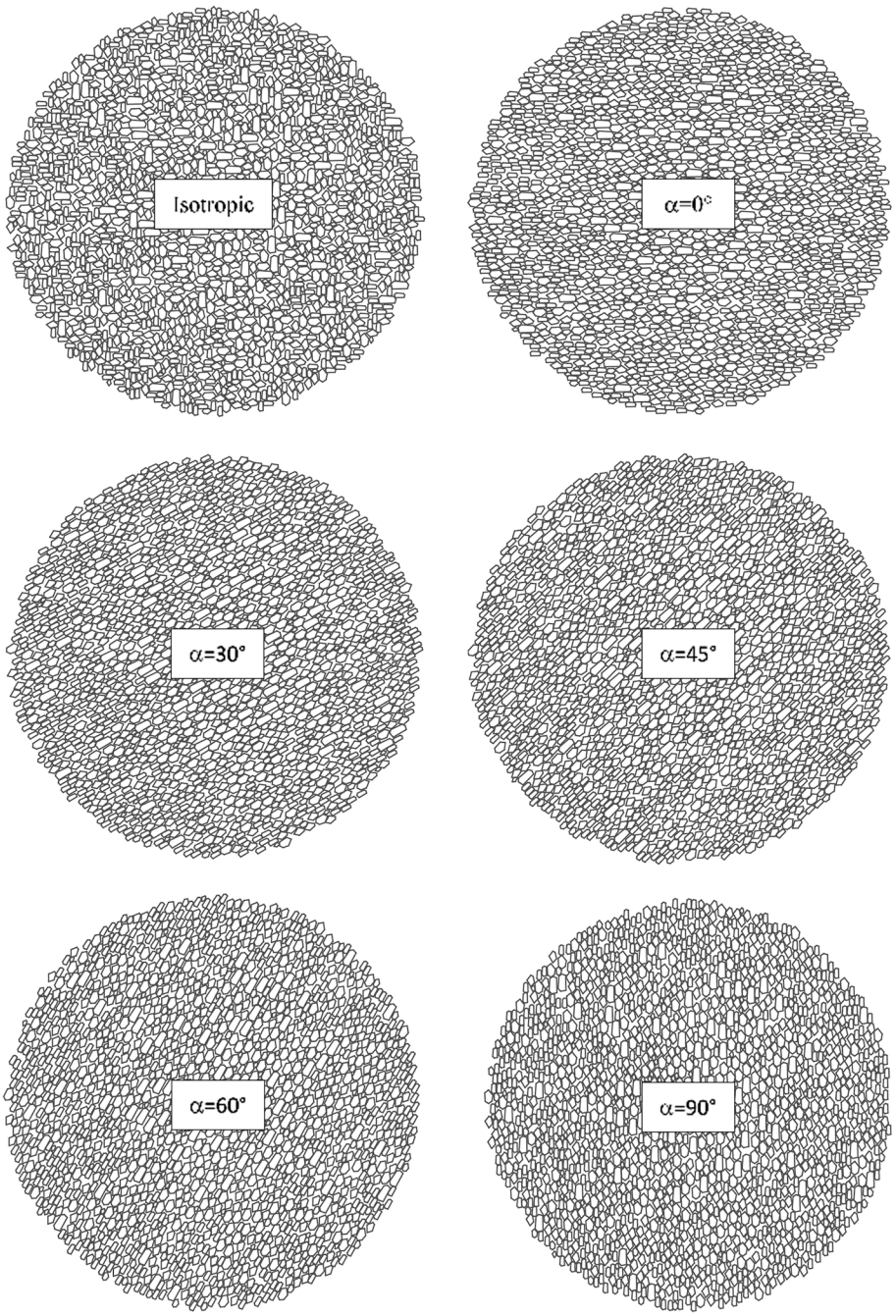

Fig. 2 Schemes of the samples used in the present study with different placement angles

inherent anisotropy angle does not favor a particular value and is close to zero.

2.3 Confinement of soil samples

Once a sample is generated, it undergoes a specific applied pressure to confine it. This compression serves as a stress-controlled mode to compact isotropically the sample. Both anisotropic and isotropic fabric samples are subjected to this confining pressure whose value should be effective to have liquefaction phenomenon. The contraction behavior of the samples is crucial to achieve liquefaction. However, the particles in the sample have sharp and elongated shapes, leading to strong interlocking and fastening, making it difficult to achieve a loose state. Consequently, the general behavior tends to be expansive rather than easily reaching a loose state. To observe the contraction behavior of the samples, various confining pressures were applied to each sample to analyze how their volume changed under biaxial loading. Ultimately, it was discovered that the samples exhibited contraction specifically at a confining pressure of $p'_0 = 700$ kPa. Alternatively, to facilitate the liquefaction of the samples, it is crucial to minimize the density of the samples and maximize their initial porosity ratio. To achieve this objective, the application of confining pressure on the samples was carried out in two distinct stages. Initially, the contact friction coefficient among the particles was set to one ($\mu = 1$). Following the initial compaction of the sample, the friction coefficient was then decreased to 0.5. To ensure equilibrium among the particles, the sample was reloaded, allowing them to move and rotate in relation to one another. This process was repeated until the sample volume reached a steady state. Figure 3 illustrates the variations in the void ratio throughout the calculation cycles. The initial void ratio of the sample was 0.605, which decreased to 0.308 after the first stage of confining loading. Eventually, with the reduction in the friction coefficient, it stabilized at a constant value of 0.28. Attaining the highest possible void ratio in these samples required multiple trials and errors. It should be noted that this value appears significantly smaller compared to real soil values. This discrepancy can be attributed to the fact that the particles used in this study are two-dimensional, resulting in smaller void ratios compared to samples with three-dimensional particles.

2.4 Simulation of undrained condition

This study addresses the undrained condition of soil samples by employing constant volume method. In this method, the effect of the fluid in a granular material is simulated by maintaining the volume of the soil constant during loading. This assumption is related to the very low compressibility of the fluid compared to the soil skeleton.

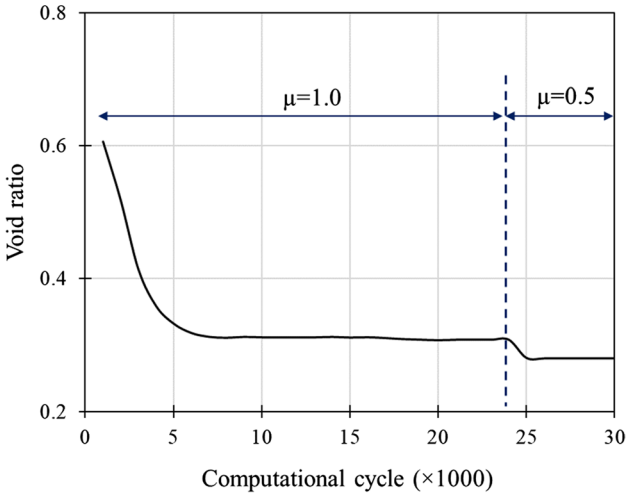

Fig. 3 Volume change in a typical sample versus the number of computational cycles

In fact, in this approach, water particles are not considered, and therefore, water is assumed to be incompressible. Instead, the boundary displacement condition of the sample is defined in such a way that the incremental axial strains in both horizontal and vertical directions are opposite, resulting in a zero volumetric strain. In comparison, the coupled method simultaneously consider water and soil particles to analyze fluid flow and particle displacement to consider the mutual effect of the fluid and particles. In this approach, not only the properties of the particles but also the properties of the fluid are taken into account. Some studies [36–38] show that the results of the constant volume method and the coupled method have relatively small differences. While the coupled method is more time-consuming and costly, the constant volume method is relatively simple and requires less time for analysis. The constant volume method have been used in many research works [37, 39–50] to simulate the static and cyclic behavior of sandy samples with circular, spherical, or elliptical particles, even in large strain deformation conditions approaching critical states.

To ensure undrained conditions during biaxial loading, where water and solid soil particles are incompressible, the displacement conditions at the sample's boundaries are defined in a manner that keeps the volume constant and thus, the volumetric strain of the sample should be kept zero. Knowing that the volumetric strain is the sum of the vertical and horizontal strain components of the sample, the boundary particles are moved horizontally such that the incremental horizontal component of the strain equals that of the applied incremental vertical strain component. More explanations concerning the concept and description of constant volume approach can be found in the reference [51].

2.5 Application of deviatoric stress

Following the completion of the consolidation stage, the samples undergo biaxial loading and are exposed to deviatoric stress. Each sample is individually subjected to both static and cyclic loading, as explained in detail below. All samples were loaded in undrained condition by using constant volume approach. Figure 4 depicts the schemes of five anisotropic samples with $\alpha = 0$, 30, 45, 60, and 90° after isotropic compaction as well as the final state of biaxial static loading stages corresponding to axial strain of 50%. Each sample undergoes axial strain in the vertical direction (or

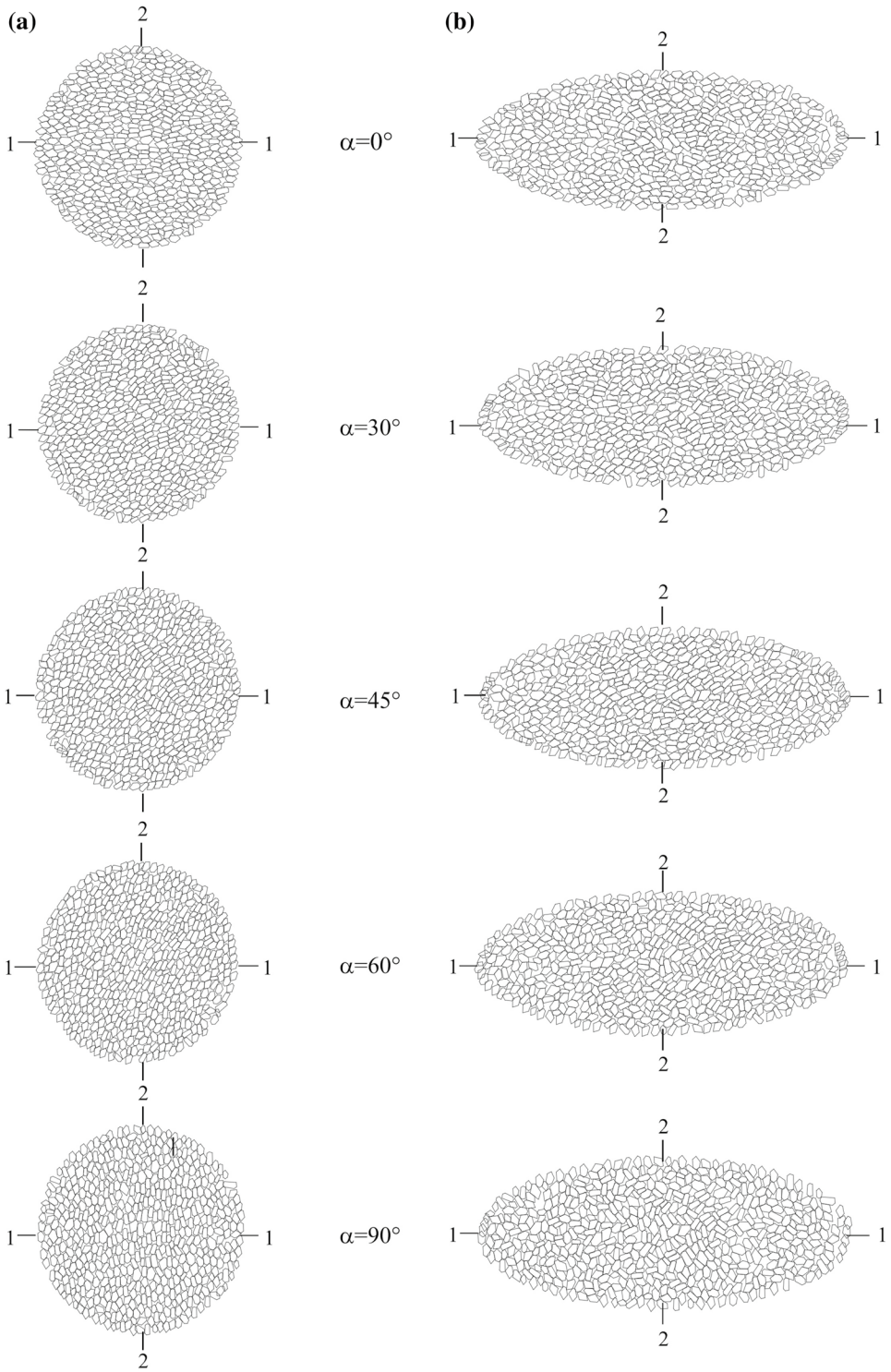

Fig. 4 Presentation of different inherently-anisotropic samples at the end of: **a** confining pressure stage; **b** deviatoric loading stage under undrained static condition (axial strain of 50%)

2–2 direction) at a consistent rate along with lateral strain in the horizontal direction (or 1–1 direction) provided that the sample volume be constant during the loading process, as already explained in the previous subsection.

Strain-controlled static loading is employed during the testing process. The boundary particles are moved toward the center of the sample by introducing a fixed vertical velocity such that each boundary particles have a vertical displacement with respect to its distance to the geometrical center of the sample. This configuration simulates the movement of two platens situated at the top and bottom of the sample. Applied vertical stress over the boundary is calculated and the difference from the lateral (horizontal) stress value is regarded as the deviatoric stress.

Cyclic loading is employed to control stress by subjecting the specimen to a consistent range of deviatoric stress along the 2–2 direction, encompassing both compression and extension directions. The loading process is defined by the stress-controlled mode. The deviatoric stress (q) is the difference between the vertical stress along 2–2 direction and that along the 1–1 direction. If the deviatoric stress reaches the desired level, the load reversal occurs and the direction of the applied boundary movement along the 2–2 direction is changed. It is reminded that the top and bottom boundary of each sample are moved vertically and the horizontal displacement of boundary particles is controlled by keeping the constant volume condition similar to what explained for static loading. To qualitatively define the cyclic loading value, Cyclic Stress Ratio (CSR) is introduced according to Eq. 1:

$$\mathrm{CSR} = \frac{q}{2p'_0} \tag{1}$$

where p'_0 represents the initial effective confining pressure applied to the sample during the compaction process in the preceding stage (=700 kPa).

2.6 Excess Pore water pressure generation

As a result of undrained conditions during cyclic loading, the sample experiences a variation in excess pore water pressure. To determine the overpressure at each loading stage in constant volume approach, the difference between the applied total stress and the effective stress of the sample is utilized in terms of confining pressure [51], as illustrated in Fig. 5. Excess pore water pressure (Δu) is determined by comparing the deviatoric stress paths of effective stress and total stress with respect to the confining pressure. The total stress path follows a straight line with a slope of 2 (vertical) to 1 (horizontal), whereas the effective stress path is curved.

In cyclic loading, the Excess Pore Water Pressure Ratio (EPWPR) named as r_u is utilized to quantify the variations

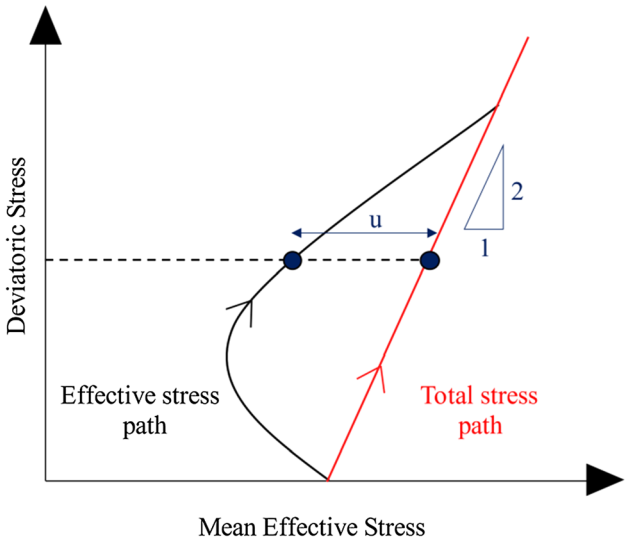

Fig. 5 Schematic demonstration of pore water pressure calculation in the constant volume method

in the generation of excess pore water pressure throughout the loading process. This ratio is calculated by dividing the excess pore pressure (Δu) by the initial effective confining pressure (p'_0):

$$r_u = \frac{\Delta u}{Po'} \tag{2}$$

The EPWPR serves as a useful indicator to identify the onset of liquefaction in cyclic loading. In technical literature, $r_u = 1$ is recognized as the threshold for initial liquefaction. At this stage, the effective stress in the soil is significantly reduced, resulting in extensive deformations and soil failure [52]. However, in recent engineering practices, efforts have been made to consider soil deformations and define liquefaction based on a strain limit. This paper adopts both approaches in defining liquefaction. In addition to the initial liquefaction approach ($r_u = 1$), a second approach is employed based on the Double Amplitude axial strain (DA). In this approach, the double amplitude axial strain is defined as the sum of the maximum and minimum axial strains in the 2–2 direction, as depicted in Fig. 6. Positive values of axial strain indicate compressive behavior of the soil, while negative strains indicate extension behavior. This study focuses on the response of the soil to axial strain with a double amplitude, where it is assumed that the behavior of the soil remains within or below five percent.

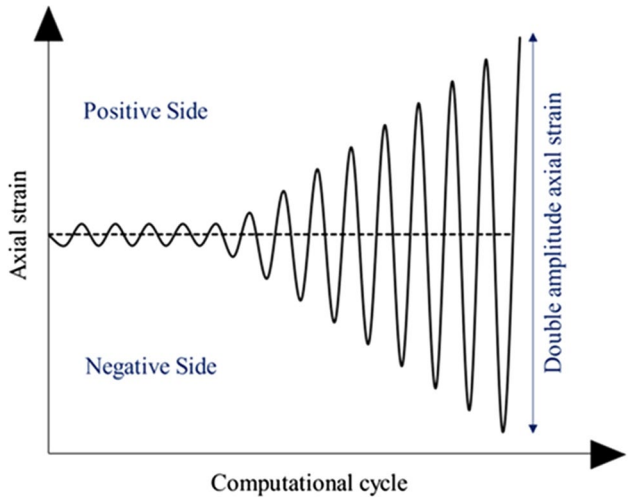

Fig. 6 Definition of Double Amplitude (DA) axial strain

3 Results of undrained static behavior

The anisotropy in the fabric of the samples has a significant effect on the shear strength of the samples under static loading and in undrained conditions. Figure 7 illustrates the outcomes of alterations in deviatoric stress relative to axial strain in the 2–2 direction (ε_{22}), as well as the stress path in the deviatoric stress versus average effective pressure space. This analysis encompasses five samples exhibiting different levels of anisotropy, alongside an isotropic sample. Biaxial loading was employed to attain the critical state, even at extensive axial strains ($\varepsilon_{22}=50\%$).

According to the observations in Fig. 7a, it is apparent that the deviatoric stress of the samples exhibits distinct patterns as the axial strain level increases. There is a noticeable deviation in the graphs at approximately $\varepsilon_{22}=3\%$. For $\alpha=0$, the deviatoric stress demonstrates an intensified increasing trend, reaching a maximum value. However, in the other samples, the growth of deviatoric stress occurs at a slower pace. Among them, the $\alpha=45°$ sample exhibits the lowest rate of deviatoric stress growth. By comparing the graphs, it can be concluded that the graph of the isotropic sample bears a closer resemblance to the $\alpha=45°$ sample graph. At very large strains ($\varepsilon_{22}>40\%$), the deviatoric stress of samples with $\alpha=0$, 30, 60, and 90° appears similar, while it is comparatively lower for the $\alpha=45°$ sample and the isotropic sample. Figure 7b provides a clearer representation of the influence of fabric anisotropy on the stress paths of the samples, as they diverge from each other right from the initial loading stage. As mentioned in Sect. 2.4, all the samples exhibit a contraction behavior. Throughout the loading process, positive pore water pressure is generated within the samples, leading to a decrease in average effective pressure. By comparing the stress paths, it can be observed that the samples with $\alpha=30°$ and $\alpha=60°$ exhibit the highest and lowest contraction behavior, respectively. Likewise, it is evident that the change trend in the isotropic sample aligns with that of the $\alpha=45°$ sample. The trend observed in this section is consistent with the findings of laboratory research conducted by Arthur and Menzies [4], Oda [5, 6], as well as numerical research conducted by Seyedi Hosseininia [22, 23], Sazzad and Suzuki [26], Mahmood and Iwashita [27], Yang et al. [28], Jiang et al.[29], Lu et al. [30], and Wang et al. [35]. These studies have all shown that the resistance of the sample decreases as the bedding angle of the particles increases, and samples with lower bedding angles exhibit a lower tendency to expand.

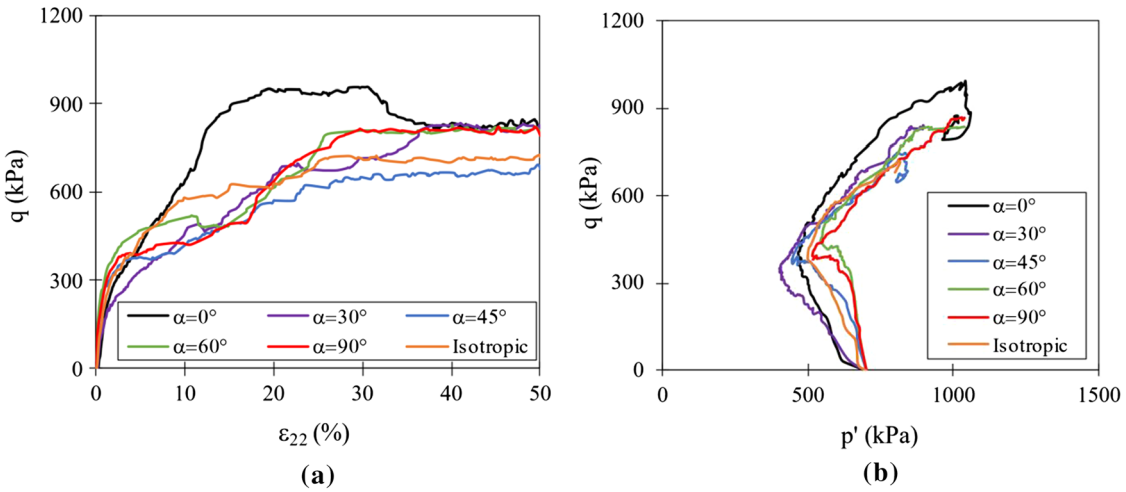

Fig. 7 Mechancial behavior of undrained samples under static loading in terms of; **a** deviatoric stress versus axial strain; **b** deviatoric stress versus mean effective stress

The parameter known as the mobilized internal friction angle (ϕ'_{mob}) is employed to examine how the presence of fabric anisotropy impacts the shear strength of samples. In the case of non-cohesive granular materials, this parameter is derived from Eq. 3, which follows the Mohr-Coulomb failure criterion:

$$\phi'_{\text{mobilized}} = \sin^{-1}\left(\frac{\sigma'_2 - \sigma'_1}{\sigma'_2 + \sigma'_1}\right) \tag{3}$$

In which, σ'_1 and σ'_2 represent the principal effective stress components in the sample. Figure 8 illustrates the variation of the mobilized internal friction angle with axial strain for samples with different bedding angles and an isotropic sample. The change patterns differ among the samples, particularly in terms of the presence of a peak. With the exception of the sample with a bedding angle of 90°, all other samples exhibit a peak in the internal friction angle. Subsequently, as the axial strain increases (around 30% onwards), the mobilized internal friction angle reaches a constant value. By definition, the maximum points on the diagram correspond to the maximum internal friction angle (ϕ'_p), and at large strains, when the value of this parameter stabilizes, the soil reaches a critical state. At this point, the friction angle can be considered as the critical internal angle (ϕ'_{cs}).

Figure 9 illustrates the relationship between fabric anisotropy and the shear strength parameter of granular materials by examining the maximum internal friction angle (ϕ'_p) and the critical state (ϕ'_{cs}) for the samples with varying bedding angles. The findings reveal that fabric anisotropy significantly influences ϕ'_p. Specifically, an increasing bedding angle corresponds to a decreasing trend in ϕ'_p. Mahmood and Iwashita [27], Lu et al. [30], and Jiang et al. [29] investigated this phenomenon using ellipsoidal particles, while Seyedi Hosseininia [22] considered sharp polygonal particles. These studies observed similar trends, with changes in f'_p aligning with variations in the bedding angle. Jiang et al. [29] demonstrated that the shear strength parameter (ϕ'_p) experiences a significant decrease when the bedding angle ranges from 15° to 75°. Conversely, the change in ϕ'_p is relatively minor when the bedding angles are between 0°–15° and 75°–90°. The research findings suggest that ϕ'_p exhibits substantial variations initially as the bedding angle increases, but the rate of change slows down after reaching a bedding angle of 45°. In comparison to Seyedi Hosseininia's work, it is observed that ϕ'_p for sharp-edged particles is higher than that for elliptical particles due to the locking effect. Despite the notable influence of fabric anisotropy on ϕ'_p, the changes in the critical state parameter ($\phi'cs$) are considerably smaller than those of ϕ'_p. However, the value of $f'cs$ is influenced by the bedding angle and is not constant, resulting in different values compared with the isotropic sample. Lu et al. [30], using the DEM and considering ellipsoidal particles, demonstrated that a constant value of ϕ'_{cs} (critical state) was obtained for all anisotropic samples. The disparity in results could be attributed to the particle shape. In Lu et al.'s study [30], elliptical particles were used, whereas this study employs polygonal and convex particles. The locking and interlocking behavior of particles in an anisotropic environment may have an impact on the soil reaching a critical state, thereby accounting for the observed differences.

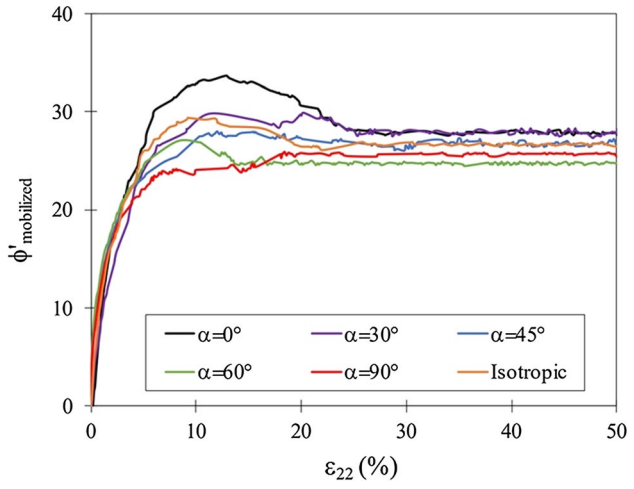

Fig. 8 The effect of inherent anisotropy on the mobilized internal friction angle under undrained condition

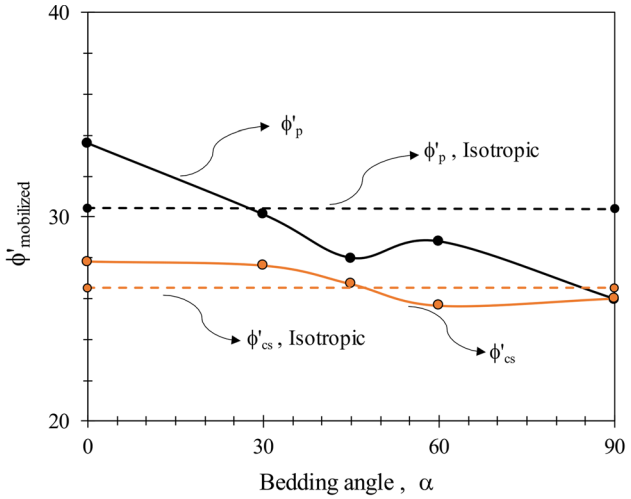

Fig. 9 Variation of peak (ϕ'_p) and critical state (ϕ'_{cs}) internal friction angles with the particle placement angles

4 Results of undrained cyclic behavior

To explore the impact of cyclic behavior on the anisotropic samples generated, both anisotropic and isotropic samples were subjected to undrained loading conditions using cyclic loading with various deviatoric stress ranges. The range of loading was defined such that CSR changes between 0.03 and 0.22. It is important to note that the loading was conducted under controlled stress conditions. Subsequently, the behavior of the samples was examined and analyzed by evaluating the variations in effective average stress, axial strain, and pore water pressure.

4.1 Stress path diagram and stress-strain diagram

Figure 10 illustrates the relationship between deviatoric stress and average effective stress for anisotropic samples at two different stress ratios of CSR = 0.071 and 0.214. In both cases, the stress path originates from the initial point $p'_0 = 700$ kPa and exhibits a zigzag pattern, initially descending in a horizontal direction. Consequently, the stress path begins as an open path, gradually transforming into

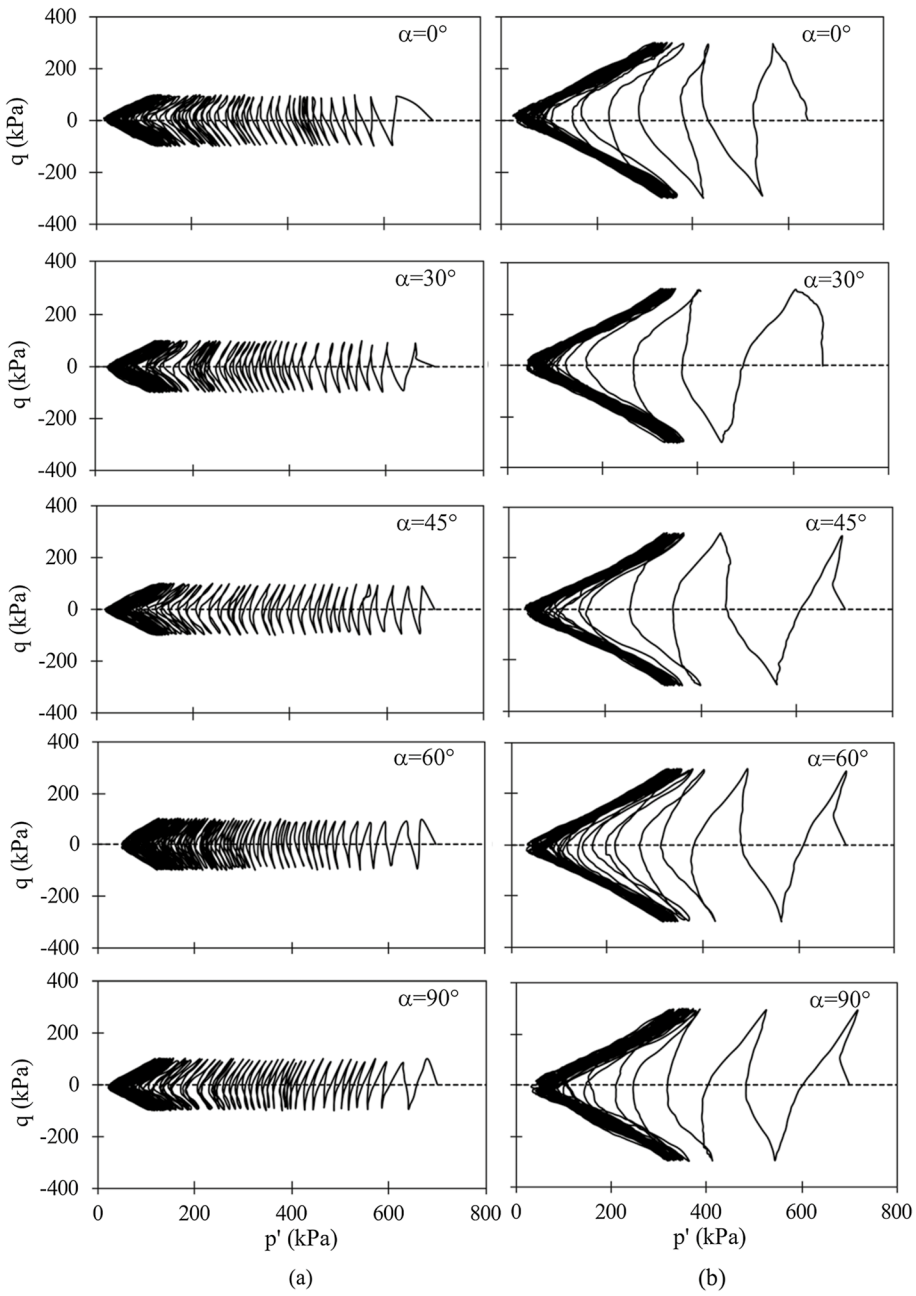

Fig. 10 Stress path diagrams for the inherently-anisotropic samples loaded under undrained cyclic biaxial test with **a** CSR = 0.071, and **b** CSR = 0.214

a butterfly shape as the average effective stress decreases. The loading cycles within the range of applied deviatoric stress follow a linear path. With the progression of loading and an increase in the number of cycles, as p'_0 decreases and approaches zero, the stress path adopts a nearly constant shape. By comparing the stress paths of samples with different bedding angles, it becomes evident that fabric anisotropy influences the number of cycles needed for the stress path diagram to reach the origin (initial liquefaction). For instance, when considering a sample with CSR = 0.214, it can be observed that the sample with a bedding angle of 60° requires more cycles to reach the origin compared to the sample with a bedding angle of 45°. Miura and Toki [8], Gao and Zhao [33], and Zhang et al. [34] conducted studies comparing the number of cycles needed for the stress path diagram to reach the origin between samples with bedding angles of 0 and 90°. Their findings revealed that the sample with a bedding angle of zero degrees reached the origin with a lower number of cycles compared to the sample with a bedding angle of 90°. Similarly, in the current research, it is evident that the sample with a bedding angle of 60° requires a higher number of cycles to approach zero effective stress compared to the sample with a bedding angle of zero. Additionally, the stress path diagram indicates that the sample with a bedding angle of 60° is further from the origin than the other samples. These observations highlight the need to further investigate the influence of the bedding angle on the number of cycles required for liquefaction, which will be addressed in more detail in Sects. 4.2 and 4.3 of the study.

Figure 11 displays the diagram illustrating the changes in deviatoric stress compared to axial strain for anisotropic samples with different bedding angles under stress ratios CSR = 0.071 and 0.214. Based on the observed findings, it is evident that the location of axial strain accumulation varies based on two factors including the magnitude of CSR and the bedding angle. At a smaller CSR value (CSR = 0.071), it can be observed that, except for the sample with a bedding angle of 45°, the concentration of axial strains is higher on the side exhibiting compressive behavior in all other samples. Moreover, the range of strains in the sample with a bedding angle of 60° is notably lower compared to the other samples, indicating a higher resistance to liquefaction. This behavioral trend differs when considering a relatively larger stress ratio (CSR = 0.214). In the case of the larger stress ratio (CSR = 0.214), the strain concentration in the sample with a bedding angle of 0° occurs on the extension side (negative deviatoric stress value), while with an increase in the bedding angle to 90°, this strain concentration shifts towards the compressive side. Laboratory research conducted by Miura and Toki [8] and Oda et al. [10] explored the trends of axial strain changes under cyclic loading with relatively large stress ratios (CSR = 0.254 and 0.305, respectively). Upon comparing these results with the findings of the present study, it can be concluded that there is a notable agreement between the laboratory results and the current research for relatively large stress ratios.

4.2 Variation of EPWPR

Figure 12 illustrates the changes in EPWPR (r_u) with the number of loading cycles for anisotropic samples under different cyclic stress ratios (CSR). Regardless of the bedding angle of the particles, it can be observed that the pore water pressure ratio in the initial loading cycle experiences a sudden increase. Subsequently, with an increasing number of loading cycles, it follows a specific trend and eventually stabilizes around $r_u = 1$. When comparing the graphs of samples with different bedding angles, it becomes apparent that the bedding angle has an impact primarily at lower CSRs, influencing the progression of r_u changes. However, as the cyclic stress ratio increases, this distinction becomes less pronounced. Figure 12 presents the results for cyclic stress ratios (CSRs) smaller than CSR = 0.107 to demonstrate the difference in behavior. In the case of CSR = 0.053, the trend of pore water pressure changes (r_u) is similar for samples with bedding angles of 30° and 45°, while the sample with a bedding angle of 60° exhibits a reduced growth of pore water pressure in the middle cycles (from the 40th cycle onwards) until it reaches a value of $r_u = 1$ in the final loading cycle (cycle number 120). The trend of r_u for the sample with a bedding angle of 90° also differs from the other samples. Similarly, for CSR = 0.071, this difference in the trend of r_u is observed, although the disparity between the graphs is less pronounced. However, for CSRs greater than 0.1, the difference between the graphs diminishes, and they nearly overlap.

The behavior of the sample in resisting liquefaction during cyclic loading can be determined by the increase in pore water pressure during the initial cycle. Laboratory findings indicate that a higher ratio of pore water pressure generated during the first cycle leads to a lower resistance to liquefaction in the sample [10]. Figure 12 illustrates the relationship between the ratio of pore water pressure generated in the first cycle and the number of cycles required for liquefaction under various cyclic stress ratios, with a double amplitude strain of 3% defined. Initially, it is evident that there is a downward trend in the change of r_u (liquefaction resistance) during the first cycle. In Oda et al.'s laboratory investigation [10], similar trends were observed as they plotted these changes for a soil sample with varying density percentages. Similarly, a downward trend was reported. Another recent laboratory study conducted by Ni et al. [16] discussed how the liquefaction resistance (r_u) changes in the first loading cycle in relation to the number of cycles required for liquefaction, and again, a downward trend was observed in the laboratory results. However, in Fig. 13, this trend is depicted

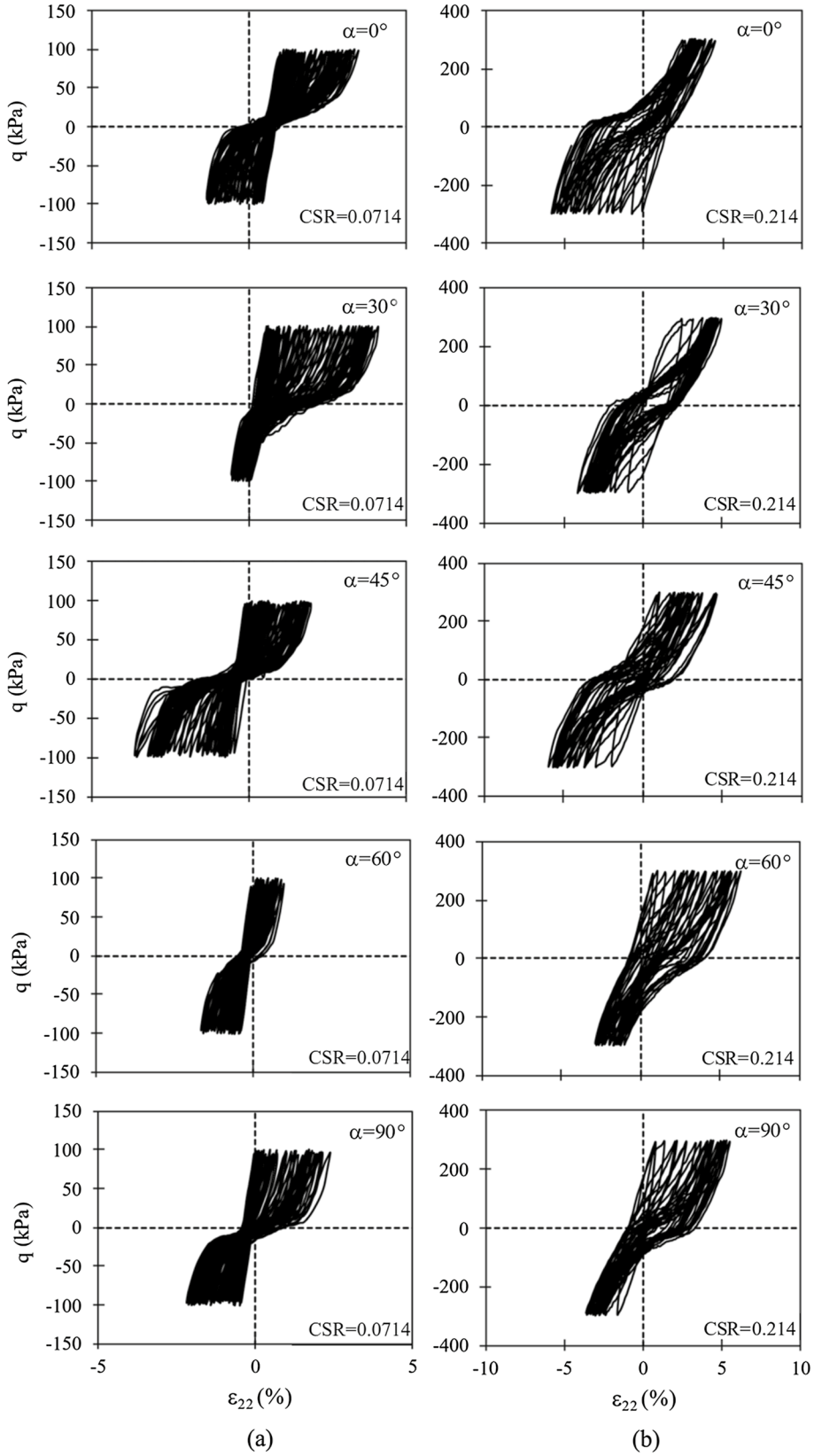

Fig. 11 Display of deviatoric stress versus axial strain diagrams of the samples under undrained cyclic biaxial test with different values of CSR: **a** CSR = 0.071 and; **b** CSR = 0.214

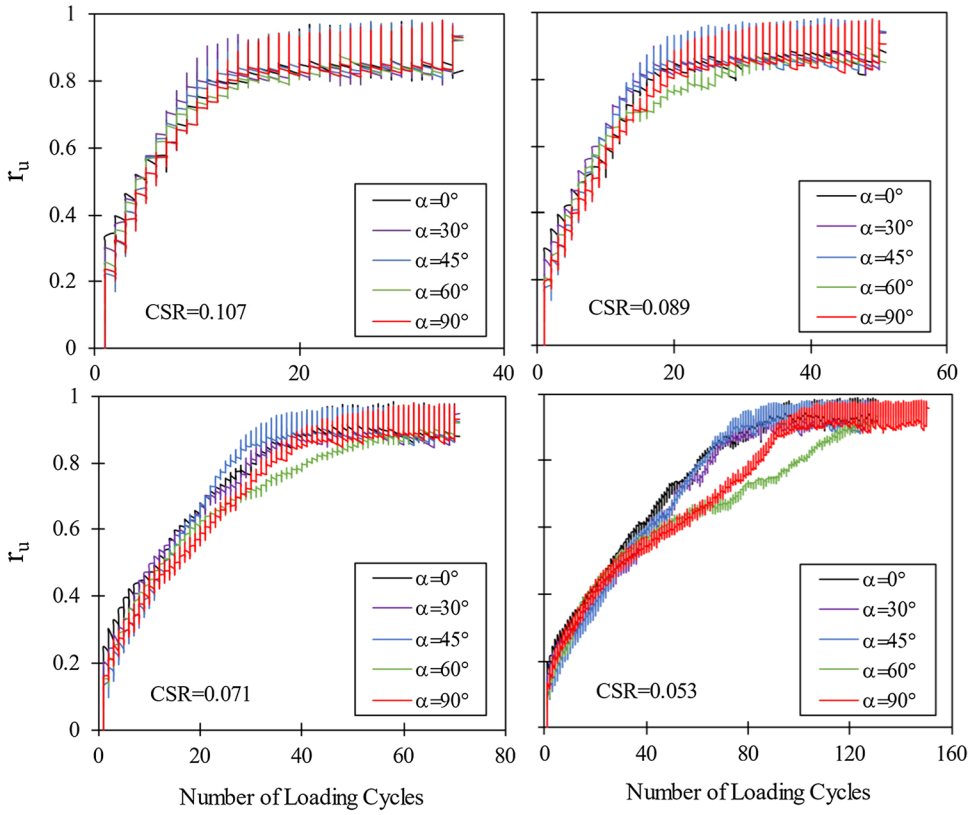

Fig. 12 Variation of r_u with No. of loading cycles with CSR values of CSR = 0.053, 0.071, CSR = 0.089, and 0.107

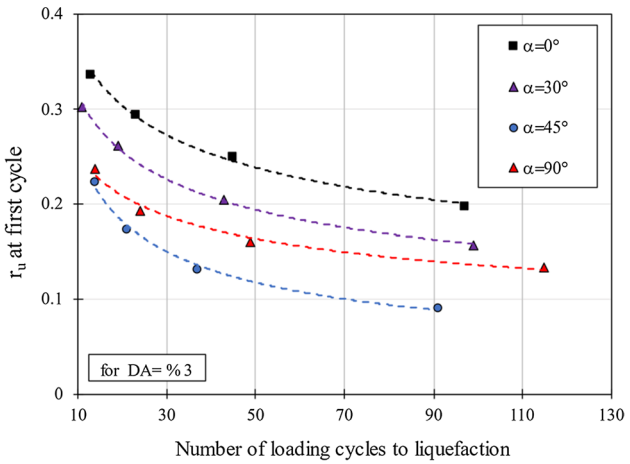

Fig. 13 Relationship between the initial value of the excess pore water pressure ratio with No. of loading cycles to liquefaction corresponding to DA = 3%

for different samples with varying bedding angles. It can be observed that the initial inherent anisotropy in the samples has a significant impact on the liquefaction resistance (r_u) during the first loading cycle. The sample with a bedding angle of zero exhibits the highest value of liquefaction resistance (r_u), while the value of r_u decreases as the bedding angle increases. Consequently, the sample with a bedding angle of 45° or 90° has the lowest value of r_u. It is worth noting that the influence of fabric on this characteristic is also observed in the laboratory findings of Ni et al. [16]. In their study, samples with the same density and stress conditions but different initial fabric resulting from various preparation methods such as moist tamping, air pluviation, and water pluviation exhibited different values of r_u and liquefaction resistance. Hence, it can be concluded that inherent anisotropy can directly impact the excess pore water pressure in the first cycle and consequently influence the resistance to liquefaction.

4.3 Effect of fabric anisotropy on cyclic liquefaction resistance

The determination of the liquefaction resistance of the samples is based on the stress and strain limits mentioned earlier in Sect. 4.2. It should be noted that liquefaction can be defined for different pore water pressure ratios other than $r_u = 1$. Figure 14 illustrates the correlation between the CSR value and the number of cycles needed to achieve r_u values of 0.95, 0.85, and 0.6. In all the samples, as the CSR value increases, the number of cycles required for liquefaction decreases. The figure indicates that this reduction process is influenced by the particle bedding angle or inherent anisotropy. By altering the bedding angle of the particles, the number of cycles needed for liquefaction varies for each sample with the same CSR value. The influence of

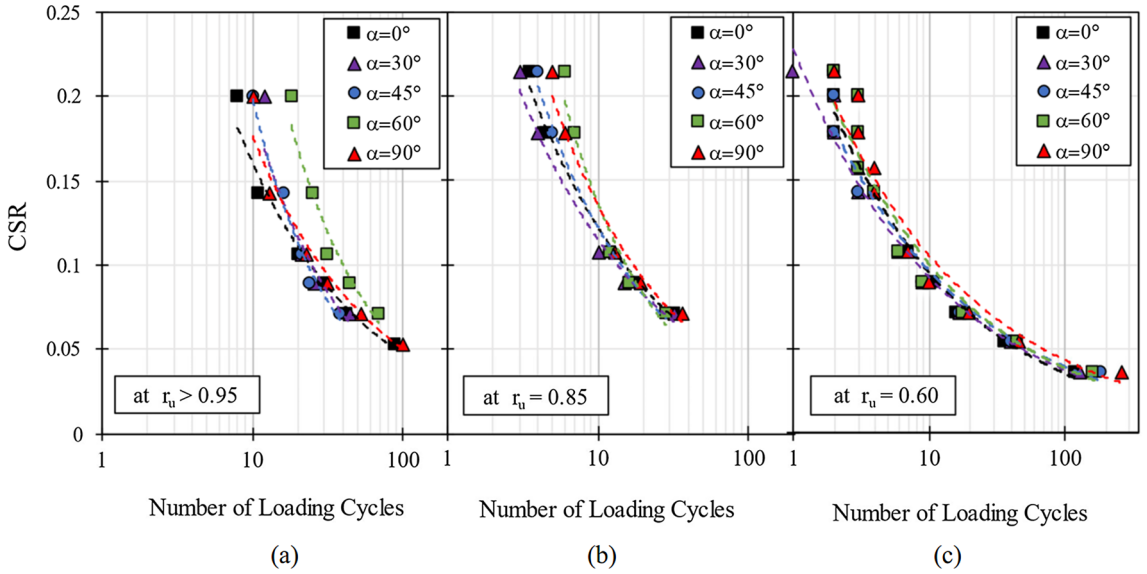

Fig. 14 Relationship between CSR and No. of loading cycles required to reach different values of r_u: **a** r_u greater than 0.95, **b** $r_u = 0.85$, **c** $r_u = 0.6$

inherent anisotropy on the initial liquefaction resistance is clearly evident based on Fig. 14a. The sample with a bedding angle of 60° exhibits the highest resistance, while the sample with a bedding angle of 0° shows the lowest resistance against initial liquefaction. These findings align well with the laboratory results of Miura and Toki [8] at $r_u = 1$. Examining Fig. 14b,c, it is observed that the impact of anisotropy becomes weaker at smaller values of r_u, resulting in a decreased separation between the graphs. At $r_u = 0.85$, the sample with a bedding angle of 60° still exhibits the highest resistance, whereas the sample with a bedding angle of 30° shows the lowest resistance. As r_u decreases further ($r_u = 0.6$), it can be concluded that nearly all the graphs overlap and display similar behavior. In essence, inherent anisotropy in the fabric appears to be influential primarily during the initial liquefaction stage ($r_u = 1$).

The impact of fabric on the liquefaction of anisotropic samples has also been examined by considering the double amplitude strain. Figure 15 illustrates the correlation between the CSR value and the number of cycles needed

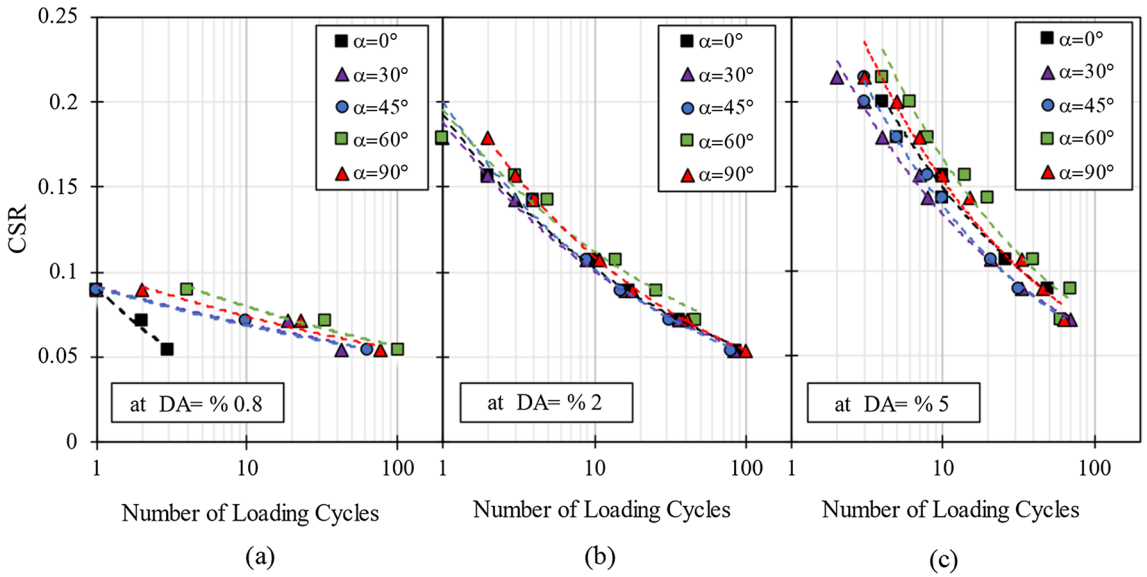

Fig. 15 Relationship between CSR and No. of loading cycles required to reach different values of DA strain: **a** DA = 0.8%, **b** DA = 2%, **c** DA = 5%

to achieve double amplitude strains of DA = 0.8, 2, and 5% in samples with varying particle bedding angles. The trend observed is that the CSR values decrease as the number of cycles required for the desired strain range increases. Moreover, larger double amplitude strains correspond to higher CSR values. Notably, the effect of inherent anisotropy in the fabric on different CSR values is more pronounced when considering different double amplitude strain levels compared to r_u. Across all double amplitude strains, the sample with a bedding angle of 60° consistently exhibits the highest CSR value. In the case of different values of the bedding angle (α), no specific trend is observed regarding the minimum CSR value based on the level of the double strain range. However, it is consistently observed that the CSR values associated with the sample having a bedding angle of 90° are always higher than those of the sample with a bedding angle of zero. This finding is in line with the experimental results previously demonstrated by Miura and Toki [8] and Oda et al. [10]. The research conducted by Oda et al. [10] also indicates that the sample with a bedding angle of 60° exhibits higher CSR values compared to the other samples. Therefore, it can be concluded that the numerical simulation results are in good agreement with the laboratory findings mentioned above.

Figure 16 compares the CSR values of anisotropic samples with bedding angles of 0.45° and 90° for two different double amplitude strains, namely DA = 0.8% and DA = 2%, based on the number of required loading cycles. The continuous lines represent the double amplitude of 0.8%, while the dashed lines correspond to the double amplitude of 2%. The shape of the data points indicates the different bedding angles. It is evident that as the bedding angle increases, the number of cycles needed to achieve the double amplitude strain also increases, resulting in an increased liquefaction resistance of the sample. Additionally, for the larger double amplitude strain (DA = 2%), the graphs depicting the CSR values are closely aligned, indicating that the influence of the fabric on the liquefaction resistance of the samples is weaker at higher double strain levels. The laboratory study conducted by Miura and Toki [8] investigated the number of cycles required to induce liquefaction for two samples with bedding angles of zero and 90° at double amplitude strains of 1, 2, and 5%. The findings revealed that the sample with a bedding angle of 90° exhibited higher liquefaction resistance. Moreover, as the double amplitude strain increased, the difference in liquefaction resistance between the samples with 0- and 90° bedding angles decreased. By comparing the results of the present research with the laboratory findings, it can be concluded that the results are consistent and aligned with each other.

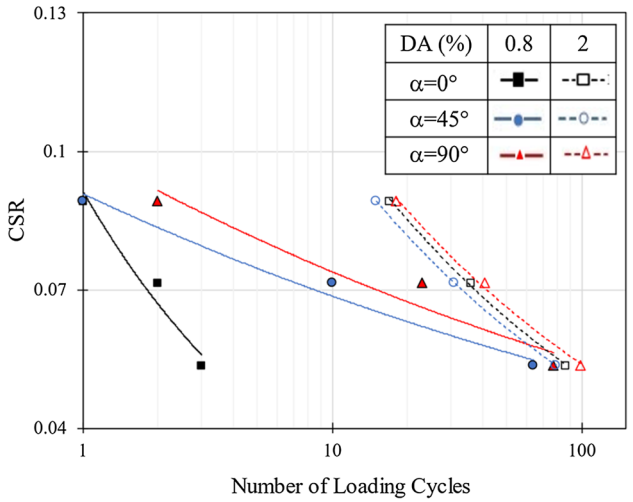

Fig. 16 Comparison of liquefaction resistance of samples with α = zero, 45, and 90° based on DA strain equal to 0.8 and 2%

5 Concluding remarks

The current study utilized the discrete element method to simulate static and cyclic biaxial compression tests under undrained condition. The soil samples consisted of elongated sharp-angled particles, and their initial fabric was varied. Specifically, the angles of the particles with respect to the horizon were set to zero, 30, 45, 60, and 90°, in addition to a sample with isotropic fabric. By analyzing the behavior of the samples and assessing their resistance against cyclic liquefaction, the following results were obtained:

- The stress paths resulting from specimens with different fabric anisotropy under undrained static loading are distinct from each other. Initial axial strain values indicate that the specimen with α = 0° exhibits the highest deviatoric stress compared to the other specimens. The deviatoric stress in the specimen with α = 45° grows at a slower rate and exhibits behavior that is almost similar to the isotropic specimen. Additionally, at very large strains ($\varepsilon_{22} > 40\%$), the deviatoric stress values for anisotropic specimens with α = 0, 30, 60, and 90° are similar to each other. However, the specimen with α = 45° and the isotropic specimen have lower deviatoric stress values than these specimens. This indicates the influence of fabric anisotropy on the mechanical behavior of the soil. Furthermore, through the analysis of the results, it was observed that as the bedding angle of particle increases up to α = 45°, the maximum internal friction angle is significantly affected, exhibiting a steep decreasing trend. Beyond α = 45°, the trend of change in the maximum internal friction angle becomes slower. However, the change in the critical internal friction angle is significantly less.

- By analyzing the stress path of anisotropic samples under cyclic loading, it becomes apparent that the initial fabric and inherent anisotropy have a noticeable impact on the behavior of the samples. Throughout cyclic loading, the effective confining stress diminishes, and the sample progressively approaches a liquefaction state. The inherent anisotropy introduces variations in the number of cycles necessary for the initial liquefaction of the sample. The specimen with $\alpha = 60°$ requires a greater number of cycles compared to the other specimens to approach zero effective stress, and it also approaches the origin of the graph less closely. Furthermore, upon examining the stress-strain diagrams, it becomes evident that fabric anisotropy can cause the concentration of compression or extension strains to shift within the sample during cyclic loading. At relatively high cyclic stress ratios (CSR = 0.214), it was observed that strain localization in the specimen with $\alpha = 0°$ is in the extension side, and as the bedding angle increases to $\alpha = 90°$, this strain localization tendency shifts towards the compression side.
- The magnitude of the cyclic stress ratio is an additional factor that influences the response of anisotropic samples to liquefaction. Through an analysis of the samples' behavior in terms of excess pore water pressure ratio, it becomes apparent that the influence of inherent anisotropy is more pronounced at lower stress ratios. As the level of the cyclic stress ratio increases, the rising trend of the excess pore water pressure ratio (r_u) in anisotropic samples becomes more similar. At CSR values of 0.053 and 0.071, it is evident that the increasing trend of r_u in the specimen with $\alpha = 60°$ is slower compared to the other specimens. However, with an increase in the magnitude of the cyclic stress ratio, this difference becomes less pronounced, and specimens with different fabric anisotropy exhibit similar behavior.
- The extent of excess pore water pressure increase in the initial loading cycle is directly linked to the resistance against liquefaction. Consequently, a higher value of the r_u corresponds to a lower number of cycles required for liquefaction to occur. The r_u value generated in the first cycle is the highest in the specimen with $\alpha = 0°$ and the lowest in the specimens with $\alpha = 45$ and 90°. This phenomenon holds true for all anisotropic samples, and by altering the bedding angle, the r_u value in the first cycle can be modified.
- Under uniform stress loading conditions (constant CSR), it has been observed that the influence of inherent anisotropy is particularly prominent during the initial liquefaction stage ($r_u = 1$). In the investigation of the inherent anisotropy's effect on initial liquefaction resistance, it was observed that the specimen with $\alpha = 60°$ exhibits the highest resistance, while the specimen with $\alpha = 0°$ shows the lowest resistance to initial liquefaction. However, if the liquefaction of the samples is evaluated at values smaller than r_u, the impact of inherent anisotropy can be disregarded or considered negligible.
- In the context of liquefaction definition, when the double strain amplitude level is considered instead of the stress criterion, the inherent anisotropy effect continues to influence the liquefaction resistance. At a specific double amplitude level, a lower cyclic stress ratio results in a reduced number of cycles required to achieve liquefaction (reaching the desired DA). In all double strain amplitude levels, the CSR value for the specimen with $\alpha = 60°$ is larger, and the CSR values associated with the specimen with $\alpha = 90°$ are consistently greater than the specimen with $\alpha = 0°$. The effect of inherent anisotropy becomes more pronounced at smaller double strain amplitude levels.

Given the time-consuming nature of simulations of cyclic mechanical behavior using the DEM method, this research opted for the use of flat two-dimensional particles for the sake of simplicity. However, it is recommended to employ 3D simulations to fully explore the effect of inherent anisotropy in the samples. Additionally, future research endeavors can leverage the DEM to investigate the microscale behavior of cyclic liquefaction in anisotropic soil, enabling a more comprehensive understanding of this phenomenon. The mechanical behavior of assemblies with initially anisotropic fabric would also be of interest for further investigation, particularly regarding the influence of particle shape and size.

Supplementary Information The online version contains supplementary material available at https://doi.org/10.1007/s10035-024-01397-4.

Declarations

Conflict of interest The authors declare that they have no conflict of interest.

References

1. Yamashita, S., Toki, S.: Effects of fabric anisotropy of sand on cyclic undrained triaxial and torsional strengths. Soils Found. **33**(3), 92–104 (1993)
2. Ashmawy, A.K., Hoang, V.V., Sukumaran, B.: Evaluating the influence of particle shape on liquefaction behavior using discrete element modeling. In: The Thirteenth International Offshore and Polar Engineering Conference 2003. OnePetro
3. Keramatikerman, M., Chegenizadeh, A.: Effect of particle shape on monotonic liquefaction: natural and crushed sand. Exp. Mech. **57**(8), 1341–1348 (2017)
4. Arthur, J., Menzies, B.: Inherent anisotropy in a sand. Géotechnique **22**(1), 115–128 (1972)
5. Oda, M.: Initial fabrics and their relations to mechanical properties of granular material. Soils Found. **12**(1), 17–36 (1972)

6. Oda, M., Koishikawa, I., Higuchi, T.: Experimental study of anisotropic shear strength of sand by plane strain test. Soils Found. **18**(1), 25–38 (1978)
7. Miura, S., Toki, S.: A sample preparation method and its effect on static and cyclic deformation-strength properties of sand. Soils Found. **22**(1), 61–77 (1982)
8. Miura, S., Toki, S.: Anisotropy in mechanical properties and its simulation of sands sampled from natural deposits. Soils Found. **24**(3), 69–84 (1984)
9. Nakata, Y., Hyodo, M., Murata, H., Yasufuku, N.: Flow deformation of sands subjected to principal stress rotation. Soils Found. **38**(2), 115–128 (1998)
10. Oda, M., Kawamoto, K., Suzuki, K., Fujimori, H., Sato, M.: Microstructural interpretation on reliquefaction of saturated granular soils under cyclic loading. J Geotech Geoenvironmental Eng **127**(5), 416–423 (2001)
11. Yang, Z., Li, X., Yang, J.: Quantifying and modelling fabric anisotropy of granular soils. Géotechnique **58**(4), 237–248 (2008)
12. Sze, H., Yang, J.: Failure modes of sand in undrained cyclic loading: impact of sample preparation. J Geotech Geoenvironmental Eng **140**(1), 152–169 (2014)
13. Wei, J., Wang, G.: Evolution of fabric anisotropy in cyclic liquefaction of sands. J Micromechanics Mole Phys **1**(03n04), 1640005 (2016)
14. Chen, Y.-C., Chuang, J.-C.: Effects of fabric on steady state and liquefaction resistance. In: The Eleventh International Offshore and Polar Engineering Conference. OnePetro (2001)
15. Yu, H., Zeng, X., Li, B., Ming, H.: Effect of fabric anisotropy on liquefaction of sand. J Geotech Geoenvironmental Eng **139**(5), 765–774 (2013)
16. Ni, X.-Q., Zhang, Z., Ye, B., Zhang, S.: Unique relation between pore water pressure generated at the first loading cycle and liquefaction resistance. Eng. Geol. **296**, 106476 (2022)
17. Cundall, P.A., Strack, O.D.: A discrete numerical model for granular assemblies. Géotechnique **29**(1), 47–65 (1979)
18. Mirghasemi, A., Rothenburg, L., Matyas, E.: Numerical simulations of assemblies of two-dimensional polygon-shaped particles and effects of confining pressure on shear strength. Soils Found. **37**(3), 43–52 (1997)
19. Seyedi Hosseininia, E., Mirghasemi, A.: Numerical simulation of breakage of two-dimensional polygon-shaped particles using discrete element method. Powder Technol. **166**(2), 100–112 (2006)
20. Seyedi Hosseininia, E., Mirghasemi, A.A.: Effect of particle breakage on the behavior of simulated angular particle assemblies. China Particuology **5**(5), 328–336 (2007)
21. Honari, S., Seyedi Hosseininia, E.: Particulate modeling of sand production using coupled DEM-LBM. Energies **14**(4), 906 (2021)
22. Seyedi Hosseininia, E.: Investigating the micromechanical evolutions within inherently anisotropic granular materials using discrete element method. Granular Matter **14**(4), 483–503 (2012)
23. Seyedi Hosseininia, E.: Discrete element modeling of inherently anisotropic granular assemblies with polygonal particles. Particuology **10**(5), 542–552 (2012)
24. Seyedi Hosseininia, E.: Stress–force–fabric relationship for planar granular materials. Géotechnique **63**(10), 830–841 (2013)
25. Seyedi Hosseininia, E.: A micromechanical study on the stress rotation in granular materials due to fabric evolution. Powder Technol. **283**, 462–474 (2015)
26. Sazzad, M., Suzuki, K.: Micromechanical behavior of granular materials with inherent anisotropy under cyclic loading using 2D DEM. Granular Matter **12**(6), 597–605 (2010)
27. Mahmood, Z., Iwashita, K.: Influence of inherent anisotropy on mechanical behavior of granular materials based on DEM simulations. Int. J. Numer. Anal. Meth. Geomech. **34**(8), 795–819 (2010)
28. Yang, Z., Yang, J., Wang, L.: Micro-scale modeling of anisotropy effects on undrained behavior of granular soils. Granular Matter **15**(5), 557–572 (2013)
29. Jiang, M., Zhang, A., Fu, C.: 3-D DEM simulations of drained triaxial tests on inherently anisotropic granulates. Eur. J. Environ. Civ. Eng. **22**(sup1), s37–s56 (2018)
30. Lu, X., Zeng, S., Li, L., Qian, J., Huang, M.: Two-dimensional discrete element simulation of the mechanical behavior and strain localization of anisotropic dense sands. Granular Matter **21**, 1–16 (2019)
31. Wei, J., Wang, G.: Discrete-element method analysis of initial fabric effects on pre-and post-liquefaction behavior of sands. Géotechnique Letters **7**(2), 161–166 (2017)
32. Bokkisa, S.V., Wang, G., Huang, D., Jin, F.: Fabric evolution in post-liquefaction and re-liquefaction of granular soils using 3D discrete element modelling. In: Earthquake Geotechnical Engineering for Protection and Development of Environment and Constructions, pp. 1461–1468. CRC Press (2019)
33. Gao, Z., Zhao, J.: Constitutive modeling of anisotropic sand behavior in monotonic and cyclic loading. J. Eng. Mech. **141**(8), 04015017 (2015)
34. Zhang, A., Jiang, M., Wang, D.: Effect of fabric anisotropy on the cyclic liquefaction of sands: insight from DEM simulations. Comput. Geotech. **155**, 105188 (2023)
35. Wang, R., Cao, W., Xue, L., Zhang, J.-M.: An anisotropic plasticity model incorporating fabric evolution for monotonic and cyclic behavior of sand. Acta Geotech. **16**(1), 43–65 (2021)
36. Liu, G., Rong, G., Peng, J., Zhou, C.: Numerical simulation on undrained triaxial behavior of saturated soil by a fluid coupled-DEM model. Eng. Geol. **193**, 256–266 (2015)
37. Shafipour, R., Soroush, A.: Fluid coupled-DEM modelling of undrained behavior of granular media. Comput. Geotech. **35**(5), 673–685 (2008)
38. Khalili, Y., Mahboubi, A.: Discrete simulation and micromechanical analysis of two-dimensional saturated granular media. Particuology **15**, 138–150 (2014)
39. Bonilla, R.R.O.: Numerical Simulations of Undrained Granular Media. University of Waterloo, Waterloo, ON (2004)
40. Dinesh, S., Sitharam, T.: Discrete element simulation of liquefaction behavior of granular soils under cyclic loading. In: CPFTEGE, December, 23–24 (2003)
41. Dubujet, P., Dedecker, F.: Micro-mechanical analysis and modelling of granular materials loaded at constant volume. Granular Matter **1**, 129–136 (1998)
42. El-Mestkawy, M.A.G.: Discrete Element Simulation for Seismically-Induced Soil Liquefaction. State University of New York at Buffalo, Buffalo, NY (1998)
43. El-Metskawy, M., Ghanem, R.: Modeling of the dynamic behavior of a probabilistic soil fabric with the discrete element method. In: Proceedings of the 8th ASCE Specialty Conference on Probabilistic Mechanics and Structural Reliability 2000, vol. 309
44. Gong, G., Zha, X.: DEM simulation of undrained behaviour with preshearing history for saturated granular media. Modell. Simul. Mater. Sci. Eng. **21**(2), 025001 (2013)
45. Khabazian, M., Seyedi Hosseininia, E.: Simulation of critical state behavior of granular soils with polygonal particles using Discrete Element Method (DEM). Amirkabir J Civ Eng **52**(3), 711–732 (2020)
46. Kishino, Y.: Quasi-static simulation of liquefaction phenomena in granular materials. In: Science on Form/3D Dynamic Morphometry for Bridge Between Structure and Function, pp. 157–174 (1990)
47. Ng, T.-T., Dobry, R.: Numerical simulations of monotonic and cyclic loading of granular soil. J. Geotech. Eng. **120**(2), 388–403 (1994)

48. Sitharam, T., Dinesh, S.: Numerical simulation of liquefaction behaviour of granular materials using Discrete Element Method. J. Earth Syst. Sci. **112**, 479–484 (2003)
49. Sitharam, T.G.: Discrete element modelling of cyclic behaviour of granular materials. Geotech. Geol. Eng. **21**(4), 297–329 (2003)
50. Soroush, A., Ferdowsi, B.: Three dimensional discrete element modeling of granular media under cyclic constant volume loading: a micromechanical perspective. Powder Technol. **212**(1), 1–16 (2011)
51. Khabazian, M., Seyedi Hosseininia, E.: Instability of saturated granular materials in biaxial loading with polygonal particles using discrete element Method (DEM). Powder Technol. **363**, 428–441 (2020). https://doi.org/10.1016/j.powtec.2020.01.013
52. Seed, H.B., Lee, K.L.: Liquefaction of saturated sands during cyclic loading. J. Soil Mech. Found. Div. **92**(6), 105–134 (1966)